ENGINEERED SURFACE CONTROL IN TURNING PROCESS

Min-Sung Hong
Department of Production Automation Engineering
Ajou University

ABSTRACT

The feasibility of generating controlled surface topographies in single-point conventional turning operations is investigated. First, a mathematical model of the surface generation process was developed. Second, in order to control the texture of the machined surface, a micro-positioning stage and the associated command generation software were designed and built. Experimental examples have shown that surface texture can be precisely controlled and is in good agreement with the theoretical predictions.

KEY WORDS

engineered surface, surface-shaping system, turning operation, higher order motions.

1. INTRODUCTION

The geometric characteristics of engineering surfaces, generated by various manufacturing processes, play a fundamental role in the prediction of the functional performance of machine components. In addition, it is known that the properties of engineering surfaces, and in particular its roughness, have great effects on lubrication, friction, etc. (Patir and Cheng, 1978).

Recently, many attempts have been made to develop numerical simulation methods for manufacturing processes. A model to predict the topography of end milled surfaces has been developed that accounts for the presence of cutter runout and deflection, and spindle speed variations (Babin, et al., 1985, 1986). In addition, a superimposed tertiary motion onto the conventional milling process has been introduced and proposed for scallop removal by considering the geometry and kinematics of the motions of the milling cutter (Hong and Ehmann, 1990; You and Ehmann, 1991). However, a more general method is still required as a tool for the evaluation of the accuracy and for the verification of the machine's performance for integrating design and manufacturing processes.

For the better understanding of the interaction between the machine tool's kinematics and the cutting tool's geometry, Hong (1994) introduced a generalized model of surface generation termed the 'surface-shaping system' which incorporates not only the nominal cutting motions but also takes into account errors during machining such as tool runout, machine deformation and vibration, as well as higher order motions. The surface-shaping system model also utilizes a precise description of the tool geometry. Therefore, this model provides a general mathematical basis for the prediction of the surface characteristics of metal-removal manufacturing processes.

The objective of this paper is to examine the feasibility of generating precisely controlled engineering surfaces in single-point cutting by building upon the principles of the surface-shaping system.

2. THEORETICAL MODEL OF SURFACE TOPOGRAPHY GENERATION

A model referred to as the 'surface-shaping system' was proposed by Hong (1994) to describe the generation and characteristics of engineering surfaces. It defines a generalized analytical framework and procedure for the simulation of surface generation processes. The model of the surface-shaping system accounts for: (a) nominal motions of the tool with respect to the workpiece, (b) a generalized representation of the complex tool geometry and of the associated errors, (c) errors caused
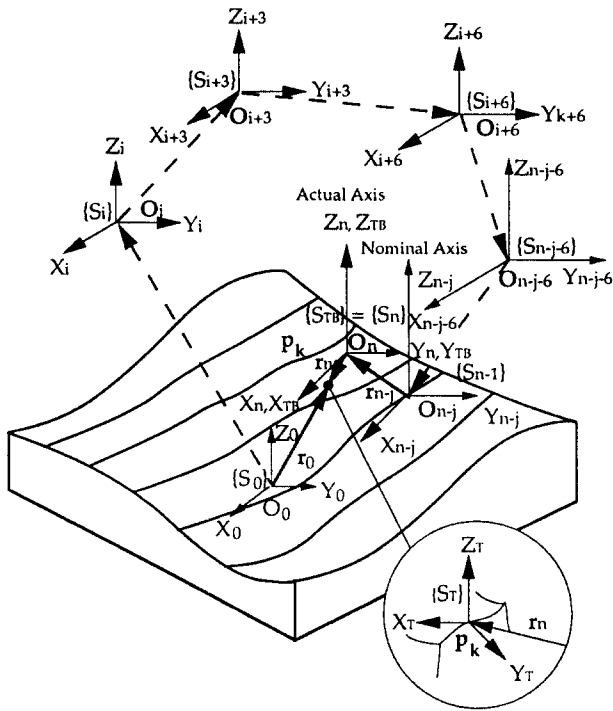
FIG. 1 COORDINATE SYSTEM AND GENERAL CUTTING
PATH OF THE SS

Cartesian coordinate systems used to describe the kinematics of the surface generation process.

The general expression for the surface-shaping points of the tool can be written as:

$$r_n = B_T \, e^4 = \prod_{i=1}^{m} A_{i-1,1}^{ji} \, e^4 \qquad (1)$$

where B_T represents a product of m matrices, A^j is the matrix of the homogeneous transformations between the tool base frame $\{S_{TB}\}$ and the tool frame $\{S_T\}$, and vector e^4 represents the origin of the tool frame.

In addition, the relation between the coordinates of points on the cutting edge in system $\{S_n\}$ and the coordinates of the same points in reference system $\{S_0\}$ of the workpiece can be written as:

$$r_0 = B_{0,n} \, r_n = \prod_{k=1}^{m} {}^@ A_{k-1,k}^{jk} \, r_n \qquad (2)$$

where the superscript $^@$ represents the characteristics of the transformation matrices A^j, i.e., nominal motions, errors, higher order motions, etc. Substituting Eq. (1) into Eq. (2), the model of the surface-shaping system is obtained as:

$$r_0 = B_{0,n} \, B_T \, e^4 \qquad (3)$$

Equation (3), the model of the surface-shaping system, links the coordinates of the surface-shaping points of the tool with the coordinates of the workpiece. A more detailed treatment of the surface-shaping system model is given by Hong (1994).

by the elastic deformation of the mechanical elements of the Machine/Fixture/Tool/ Workpiece (MFTW) system, (d) errors caused by machine tool vibrations, and (e) higher order motions used to control the desired surface texture. In this study the surface-shaping system model in conjunction with higher order (tertiary) motions will be utilized to predict and generate different surface topographies. It will be interesting to examine the capability of generating different surface topographies through different tertiary motions and cutting conditions, respectively. The surface-shaping system model will be utilized to establish a specific analytical model of surface generation in turning.

2.1 Model of the Surface-Shaping System

This model establishes a relationship between the surface-shaping points on the cutting tool and the workpiece to accurately predict the texture of the resultant machined surfaces. In order to generate the general tool path equation which defines the relationship between the cutting tool and the workpiece, a suitable set of coordinate systems is established. Figure 1 schematically shows the right-hand

2.2 Surface Generation in Turning

Figure 2 shows a turning operation with a single-point cutting tool. From Eq. (2), the radius vector r_0 of the surface-shaping points of the tool in the reference frame $\{S_0\}$ can be derived as follows:

$$r_0 = {}^N A^6(\theta) \; {}^N A^1(x) \; {}^N A^2(y) \; {}^N A^3(z) r_4 \qquad (4)$$

nose be an arc with a radius r. Then, the radius vector $\mathbf{r}_4$ of the surface-shaping points $\mathbf{p}_k$ on the cutting edge can be written as:

$$\mathbf{r}_4 = {}^{N}\mathbf{A}^{5}(\psi)\ {}^{N}\mathbf{A}^{1}(\rho)\ {}^{N}\mathbf{A}^{2}(p_{yk})\ \mathbf{e}^{4} \qquad (5)$$

where ${}^{N}\mathbf{A}^{5}(\psi)$ is the nominal rotation of the radius vector $\mathbf{r}_4$ about the Y-axis and ${}^{N}\mathbf{A}^{1}(\rho)$ and ${}^{N}\mathbf{A}^{2}(p_{yk})$ are the nominal translations ρ and p_{yk} of the radius vector $\mathbf{r}_4$ in the direction of the X and Y axes with respect to frame $\{S_4\}$, respectively. After some manipulation, the matrix form of the nominal tool path equation of the surface-shaping points $\mathbf{p}_k$ in frame $\{S_0\}$ of the turning process can be expressed as:

$$\begin{bmatrix} X_0 \\ Y_0 \\ Z_0 \end{bmatrix} = \begin{bmatrix} x\cos\theta - y\sin\theta - p_{yk}\sin\theta + \rho\cos\theta\cos\psi \\ x\cos\theta + y\cos\theta + p_{yk}\cos\theta + \rho\sin\theta\cos\psi \\ F_z t - \rho\sin\psi \end{bmatrix} \qquad (6)$$

FIG. 2 SURFACE-SHAPING SYSTEM OF THE TURNING PROCESS

where ${}^{N}\mathbf{A}^{6}(\theta)$ represents the nominal rotation of the frame $\{S_1\}$ about the Z-axis and ${}^{N}\mathbf{A}^{1}(x)$, ${}^{N}\mathbf{A}^{2}(y)$, and ${}^{N}\mathbf{A}^{3}(z)$ are the nominal translations x, y, and z of the different frames in the X, Y, and Z directions with respect to frame $\{S_0\}$, respectively. Note that $z = F_z t$, where F_z is the feedrate in the Z direction, and that $\mathbf{r}_4$ is the radius vector of the surface-shaping points of the tool in frame $\{S_4\}$.

Figure 3 shows in detail the cutting tool geometry in a turning process. In the simplest case, shown in the figure, the cutting edge along the cutter nose is the main engaged cutting edge during surface generation. When it is assumed that the tool face (A_γ) is a plane and the tool flank (A_α) is a cylindrical surface, then the cutting edge $\mathbf{p}_k$ is defined by a plane/surface intersection. Let the cutting edge on the cutter

In addition to the nominal motion described by Eq. (4), to affect and control the surface texturing processes one can superimpose higher order motions onto the nominal cutting motions. Let the general expression for higher order motions in the X-, Y- and Z- directions be defined by $h_{mx}(t)$, $h_{my}(t)$, and $h_{mz}(t)$, respectively, then, Eq. (4) can be rewritten as:

$$\mathbf{r}_0 = {}^{N}\mathbf{A}^{6}(\theta)\,{}^{N}\mathbf{A}^{1}(x)\,{}^{N}\mathbf{A}^{2}(y)\,{}^{N}\mathbf{A}^{3}(z)\,{}^{H}\mathbf{A}^{1}(h_{mx}(t))$$
$${}^{H}\mathbf{A}^{2}(h_{my}(t))\,{}^{H}\mathbf{A}^{3}(h_{mz}(t))\,\mathbf{r}_7 \qquad (7)$$

where $\mathbf{r}_7$ coincides with $\mathbf{r}_4$ in Eq. (5). Consequently, the path equation of the surface-shaping point $\mathbf{p}_k$ of the single-point cutting tool in frame $\{S_0\}$ with higher order motions can be expressed as:

$$\begin{bmatrix} X_0 \\ Y_0 \\ Z_0 \end{bmatrix} = \begin{bmatrix} \{x + h_{mx}(t)\}\cos\theta - \{y + h_{my}(t)\}\sin\theta - p_{yk}\sin\theta + \rho\cos\theta\cos\psi \\ \{x + h_{mx}(t)\}\cos\theta + \{y + h_{my}(t)\}\cos\theta + p_{yk}\cos\theta + \rho\sin\theta\cos\psi \\ F_z t + h_{mz}(t) - \rho\sin\psi \end{bmatrix} \qquad (8)$$
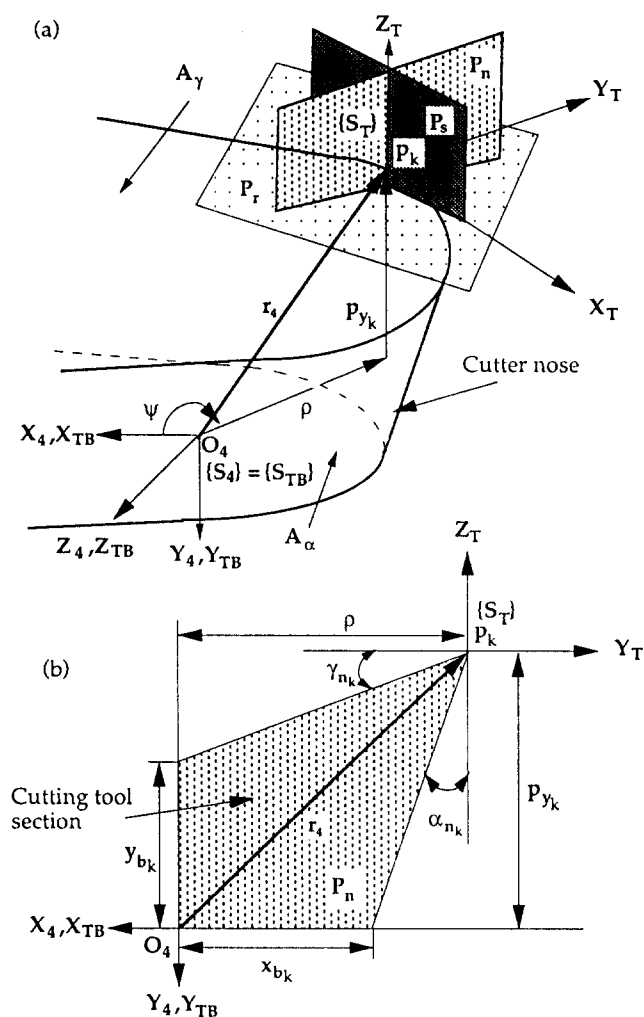
(a)

(b)

FIG. 3 (a) CUTTER NOSE OF THE SINGLE-POINT TOOL
(b) SECTIONAL VIEW OF CUTTER NOSE

Thus, Eq. (8) represents the general surface-shaping model of a single-point cutting operation that includes the cutting tool geometry and the higher order motions. Practical implementations of certain higher order motions will be discussed in Section 5.

3. PHYSICAL REALIZATION OF A SURFACE TEXTURING SYSTEM

In order to investigate the pragmatic aspects of the dynamic generation of controlled surface topographies, based on the foregoing theoretical background, the experimental system shown in Fig. 4 was developed. The essential elements are: (a) a micro-positioning stage (MPS), (b) a conventional turning system with spindle position feedback, and (c) a computer control system. In the process, the controlled surface
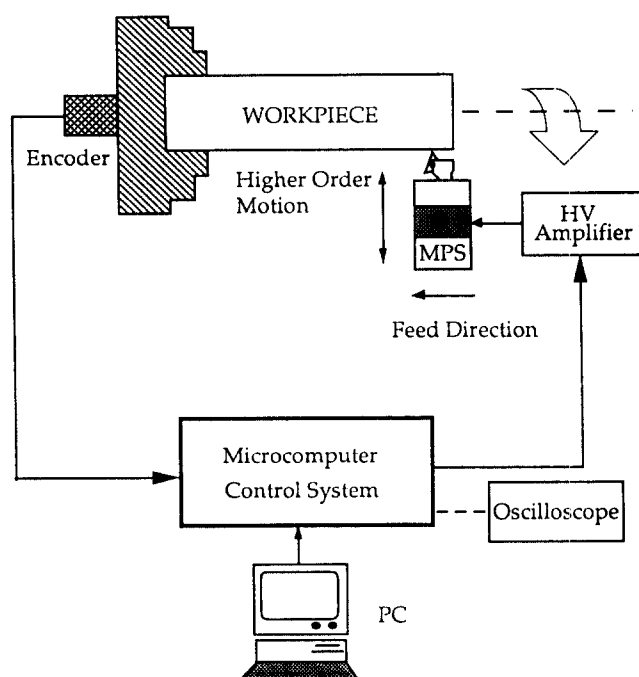

FIG. 4 SCHEMATIC DIAGRAM OF THE SURFACE TEXTURING SYSTEM

topography is imparted by a single-point cutting tool in conjunction with a suitable tertiary motion performed in the X-direction, i.e., normal to the workpiece. Each of these elements will be described in detail in the sequel.

3.1 Design, Analysis, and Testing of a Micro-positioning Stage

In recent years, a number of tool positioning systems that utilize PZT actuators have been developed for variable depth machining (Rasmussen, et al., 1992), micro-grinding (Mitzutani, et al., 1990; Zhong and Nakagawa, 1991), lithography (Moriyama, et al., 1988; Goto and Sasaoka, 1988), precise measurement of linewidths of photomasks (Scire and Teague, 1978; Katoh, et al., 1984), etc. The conventional single-axis flexure hinge, constituting the fundamental building block of these devices, was initially developed by Paros and Weisbord (1965) and they have been widely used ever since.

In this work, a compound micro-positioning stage consisting of a parallel springlike stage, a piezoelectric actuator element and a single-point cutter was designed and built. The basic design requirements were dictated by the need for high frequency and high fidelity controlled motions in the 1 to 50 μm range. The piezoelectric actuator used was a model P-243.20 made by Physic Instrumente Co. capable of generating 20,000 N of force within a 0-30 μm range at a maximal operating voltage of -1500 V. The tool used was a Kennametal cutting tool with a triangular insert # TNMG 331K. The monolythic stage was made of spring steel by a wire cut electric discharge machining. The basic design was developed by using geometric construction through a CAD system (SDRC's IDEAS VI) as shown in Fig. 5a.

Theoretical Analysis of the MPS. The MPS uses parallel springs proposed by Katoh (1984). Figure 5b shows the essential dimensions of the parallel springs with semicircular flexure hinges (Hara, et al., 1990). The force, F, needed to bend the stage by an angle θ is:

$$F = \frac{4K_B d}{l^2} = \frac{8Ebt^{5/2}d}{9l^2 R^{1/2}\pi} = K_s d \qquad (9)$$

where F is the force required to displace the parallel springs over the distance d, K_B and K_s are the torsional stiffness and stiffness of the stage, respectively, E is Young's modulus, and the length between two hinge centers, l, is equal to $(H + 2R)$. The resonant frequency of the stage, corresponding to the stage's stiffness, depends on the values of R and t and is given by:

$$K_s = \frac{8Ebt^{5/2}}{9l^2 R^{1/2}\pi} = \frac{8Eb}{9\pi\{2(R/t)+(H/t)\}^2 (R/t)^{1/2}} \qquad (10)$$

In the design process the key geometric quantities, R and t, were determined by the use of the above equations in combination with
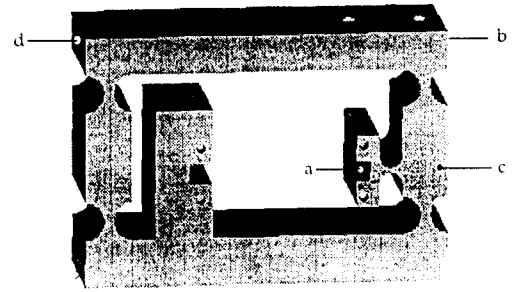
(a) MPS Structure from IDEAS VI - CAD System
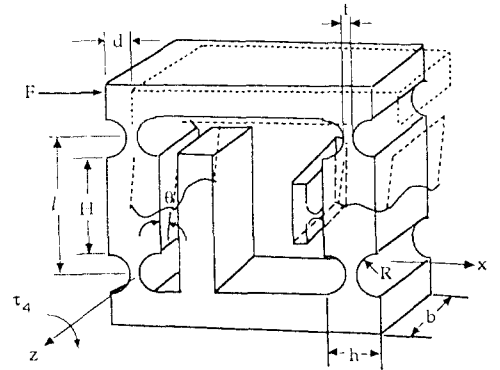
(b) Parellel Spring

FIG. 5 THE PARALLEL SPRING STAGE

FEM analysis (through SDRC's IDEAS VI). Both static and dynamics analysis were performed by using solid linear brick elements.

In the static analysis, a constant displacement 10 μm was applied at point 'a', see Fig. 5a, resulting in a deformed displacement of 17.3 μm at point 'b' yielding a 1.73 displacement gain.

For dynamic analysis the MPS was restrained at the base of the stage and a force was applied at point 'a' in the X-axis direction resulting in a natural frequency of $\omega_n = 484.59$ Hz.

Experimental Analysis of the MPS. For verifying the FEM and analytical results, both static and dynamic experiments were performed. In the static tests, the stage's stiffness, displacement gain, and the output displacement corresponding to various input command voltages were obtained. In the dynamic tests the stage's natural frequency and

response to a series of sinusoidal excitation forces were evaluated.

The static tests were performed by applying forces at point 'b' (in Fig. 5a) through a force ring, and measuring the displacements by a dial gauge at point 'd'. The experimental displacement gain of 1.75 is very close to the analytical result of 1.73. The stiffness of the stage was determined to be 371.99 N/mm as obtained from a series of tests. The maximum output displacement as a function of input voltage to the actuator of the MPS is around 30 μm generated by a -800V input voltage.

The dynamic characteristics of the MPS were measured by shock excitation in conjunction with the Fast Fourier Transform (FFT) method. An impact force was applied at point 'd' of the stage and the accelerometer was placed at point 'b' to detect the response. The transfer function was experimentally obtained by an FFT analyzer. Once again a close agreement between the experimental and analytically predicted behavior was obtained.

3.2 Turning Process with Feedback

A rotary incremental optical encoder was mounted to the end of the spindle of a conventional engine lathe. The principal function of the encoder is to provide interrupts to the control computer at equal angular intervals to facilitate a precise control of the surface features around the circumference. The relation between the arc length, l_c, and encoder resolution, N_r expressed in pulses per revolution, is:

$$l_c \approx R\Delta\theta = \frac{R2\pi}{N_r}$$ (11)

where R is the radius of the workpiece, and N_r is the total number of encoder counts per revolution.

In repetitive tool oscillations, such as sinusoidal motion, for example, the arc length of a single wave, p_l, can be obtained as:

$$p_l = N_s l_c$$ (12)

where N_s is the number of angular increments per wave, e.g., the number of encoder counts, per sinusoidal wave.

3.3 Computer Control System

To generate the desired surface topography suitable command sequences need to be generated and executed by the control computer. The hardware used in the developed system consisted of a Motorola 68020 based computer in conjunction with A/D and D/A converters and interrupt circuitry. In addition an IBM PC based system was used for off-line analysis and evaluations. Since the command sequence is a key factor defining the resulting surface it will be treated in detail in the next section.

4. COMMAND GENERATION

In conventional cutting processes, the surface topography is basically determined by the tool geometry and nominal tool motions. The tertiary motion of the cutting tool, as proposed in Section 2, introduces an important factor influencing surface topography and allows the generation of controlled patterns. The generation of the desired topography requires, however, the formulation of appropriate commands to the MPS. In this study, two types of cutting motion commands will be considered:

I) *Simple-cutting motions:* This type of command will be mainly used for generating indentations (holes) on the surface of the workpiece. The employed tertiary motion during machining is a simple repetitive motion and there is no overcut between adjacent cutting paths. The cutting operation can be either continuous or interrupted.

II) *Compound-cutting motions:* In addition to performing simple-cutting motions, various types of tertiary motions can be employed in the same cutting process. In this study, I introduce this method in combination with overlapping

adjacent cutting paths to generate 'hill' and 'hill & valley' like patterns on the machined surface.

An additional factor which needs to be considered is related to the phase shift of the resultant patterns between adjacent revolutions. This is determined by the ratio of the circumferential length of the workpiece to the unit length per single pattern feature. The phase shift produced during continuous motion is a 'natural phase shift', while the phase shift generated by resetting the tertiary motions is a 'controlled phase shift'.

For simplicity in the sequel I will assume simple sinusoidal tertiary motions to investigate the feasibility and flexibility in generating various surface textures by both simple- and compound tertiary cutting motions.

4.1 Sinusoidal Tertiary Motions

Equations (7) and (8) express the radius vector of the surface-shaping points of the tool with higher order motions in the X-, Y- and Z-directions, respectively. If for simplicity, only a tertiary sinusoidal motion in the X-direction is performed, one has:

$$
\begin{aligned}
h_{mx}(t) &= G\sin(\omega t) \\
h_{my}(t) &= 0 \\
h_{mz}(t) &= 0
\end{aligned}
\tag{13}
$$

where G is the magnitude and ω is the frequency of the sinusoidal motion, by relating this motion to the angular position of the workpiece, the first equation above becomes:

$$
h_{mx}(\omega) = G\sin\left(\frac{\omega}{\omega_s}\theta\right)
\tag{14}
$$

where ω_s is the angular velocity of the workpiece and θ is the angular position.

Taking into account encoder feedback signals, i, corresponding to a constant angular sampling interval $\Delta\theta$, Eq. (14) can be rewritten as:

$$
h_{mx}(i) = G_i\sin\left(i\frac{2\pi\omega_m}{\omega_s}\Delta\theta\right)
\tag{15}
$$

where ω_m is the frequency of the cutting tool motions.

The relationship between ω_m and ω_s can be expressed as:

$$
\omega_m = \frac{\omega_s}{N_s\Delta\theta}
\tag{16}
$$

4.2 Command Generation Process

The command generation process is controlled by the angular position of the workpiece (the encoder). The characteristics of the texture are determined by the wave length of a single sinusoidal wave, p_l, the circumferential length of the workpiece, L, and the command frequency of the MPS, ω, which is proportional to the rotational speed of the workpiece, V_r. In addition, the feedrate per revolution, f_d, determines whether or not adjacent cutting paths overlap. Various combinations of these factors result in a wide spectrum of surface topographies.

In this paper a type of command, which provides the surface texture by the combination of two different sinusoidal motions and of a constant depth cutting motion, is introduced. This command structure generates 'hill & valley' type patterns resembling the surface topography of a laser-textured surface. Three different cutting motions in the X-direction, (Fig. 6a), depending upon the revolution number, j, are used. The command equation is:

$$
h_{mx}(i,j) = G_{ij}\left\{\delta_{ij}\left[\frac{1}{2}\sin\left(\frac{2\pi i}{N_s}+\frac{\pi}{2}\right)-\frac{1}{2}\right]+1\right\}+h_{ij}
\tag{17}
$$

When $j = 3n+1$, then $G_{ij} = G_1$, $\delta_{ij} = 0$ and $h_{ij} = 0$. The cutting motion is a constant depth motion. When $j = 3n+2$, $G_{ij} = G_2$, $\delta_{ij} = 1$ and $h_{ij} = G_1$. The cutting motion is a sinusoidal motion with the maximum cutting depth equal to G_1+G_2

and the minimum cutting depth equal to G_1. When $j = 3n+3$, $G_{ij} = G_1$, $\delta_{ij} = 1$ and $h_{ij} = 0$. The cutting motion is a sinusoidal motion with the maximum cutting depth equal to G_1 and the minimum cutting depth equal to 0.

These three elementary cutting motions are sequentially repeated. Hills and valleys are generated in adjacent revolutions as shown in Fig. 6b. In this case, the traverse length between two hills (valleys) in the feed direction is $3f_d$. Similarly to the previous two types of surface generation, it is necessary to take into account η to determine the phase shift.

When η is an integer, the cutting motion is always continuous and the phase shift of the resultant patterns is zero as shown in Fig. 6b. When η is not an integer, however, each unit motion is terminated at the last cutting point of a revolution and reset to the next cutting motion at the starting point of the new revolution. Therefore, the cutting motion is discontinuous at the intersection point of two successive revolutions. A controlled phase shift can be generated by extending the cutting distance, δ_ε, during the constant depth cutting motion as shown in Fig. 6c.
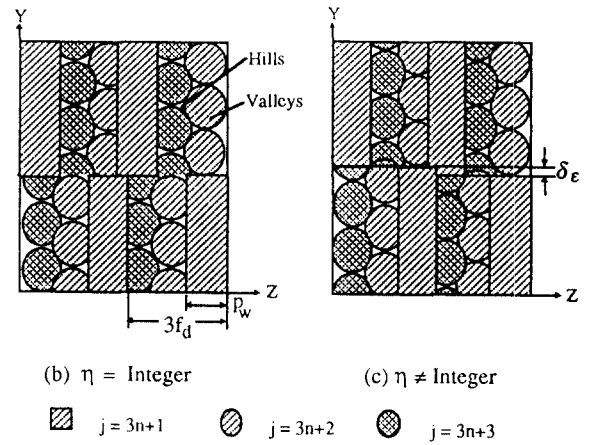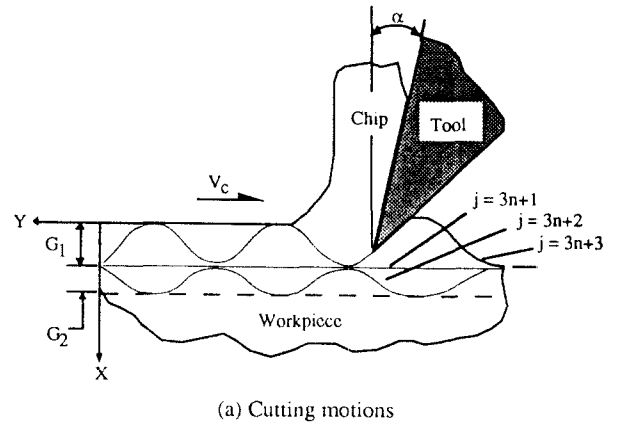
5. SIMULATION AND EXPERIMENTAL RESULTS

The purpose of this Section is to present a comparative assessment between theoretical simulations and physically generated surface topographies.

5.1 Simulation Results

Surface topography by single-point cutting was simulated based on the theoretical surface-shaping system with superimposed tertiary motions, $h_{mx}(t)$, normal to the surface of the workpiece. The tool geometry used in this simulation was: tool nose angle $\beta = 60°$, tool nose radius $\rho = 0.397$ mm, and rake angle $\alpha = 0°$, while the remaining parameters are given in Table 1. The obtained simulated surface topography is shown in Fig. 7a and the profile at the location corresponding to the maximal cutting depth is shown in Fig. 7b.

(a) Cutting motions

(b) η = Integer   (c) $\eta \neq$ Integer

▨ $j = 3n+1$ ◍ $j = 3n+2$ ◉ $j = 3n+3$

FIG. 6 SCHEMATICS OF SURFACE GENERATION THROUGH THE COMPOSITION OF THREE CUTTING MOTIONS

TABLE 1. SIMULATION AND EXPERIMENTAL PARAMETERS

		cutting depth d_c (μm)	feed d_f (μm/rev)	workpiece diameter D (mm)	command frequency ω_m (Hz)	spindle speed n (rpm)
sine wave 2	min.	0				
	max.	10				
sine wave 1	min.	10	99	36	194	31
	max.	15				
constant depth cutting		10				

5.2 Experimental Verification

Numerous experimental tests have been made to confirm the feasibility of the proposed method. A surface texturing experiment was conducted on a conventional lathe. The cutting conditions for this experiment was identical to that of the simulation. The workpiece material was brass (73.8 RB). The encoder resolution, N_r, was 4096 pulses per revolution. Table 1 also shows the working conditions for the surface generation experiment.

By using a composition of motions, a surface topography consisting of hills and valleys can be generated. Figure 8a shows a plane view photograph of the obtained surface topography. The profile corresponding to

maximal cutting depth is shown in Fig. 8b. This type of controlled surface generation produces surface features which are very similar to the patterns and the size of typical laser-textured surfaces.

This proposed example relates only to a simple type of surface topography. It is possible to obtain many other types of surfaces machined by different cutting tool geometries accompanied by desired tertiary motions.
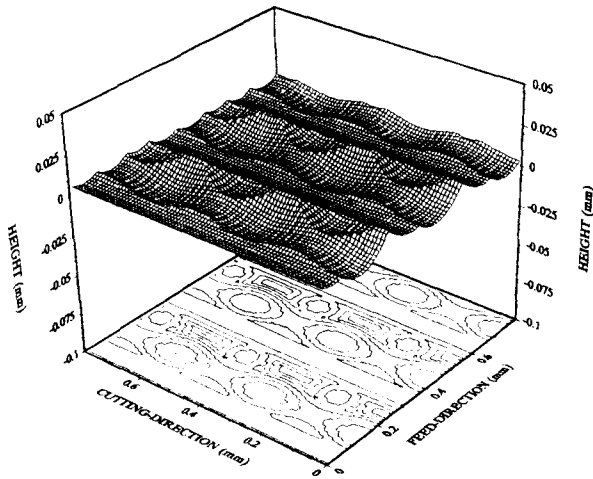
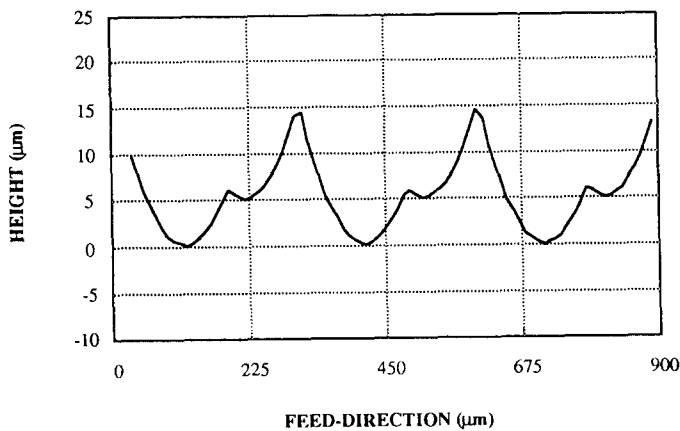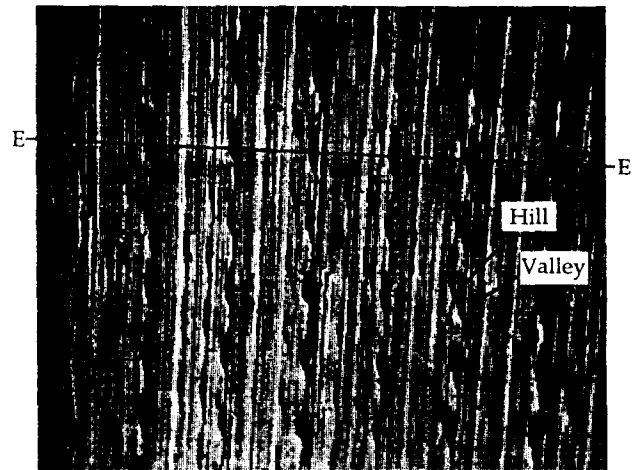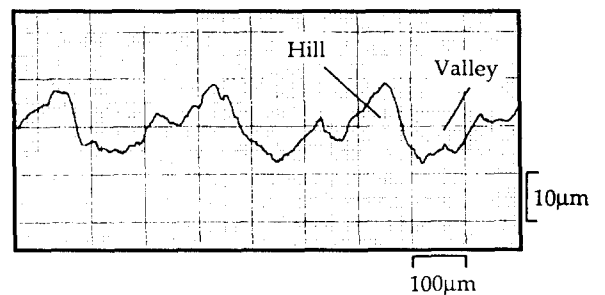FIG. 7 (a) SIMULATED SURFACE

FIG. 7 (b) THEORETICAL PROFILE AT THE MAXIMUM DEPTH

(a) PLANE VIEW PHOTOGRAPH

(b) SURFACE PROFILE

FIG. 8 SURFACE WITH HILL AND VALLEY LIKE PATTERNS

6. CONCLUSIONS

Based on the theoretical and experimental results, the following conclusions can be drawn:

(1) By using the general model of the surface-shaping system, the theoretical background for the simulation and generation of controlled surface topographies under various cutting conditions and tool geometries has been developed for turning operations. The tool geometry, kinematics of motions and tertiary motions are integrated to predict and analyze surface texture.

(2) An experimental procedure has been developed, and the necessary hardware built, to generate controlled surface topographies by using the single-point cutting method with tertiary motions. Surface patterns, including phase and size, can be precisely controlled.

(3) A series of single-point cutting tests was conducted to confirm the simulation results and investigate the characteristics of machined surfaces. The experimental results were found to be consistent with the predictions.

REFERENCES

1) Babin, T. S., Lee, J. M., Sutherland, J. W., and Kapoor, S. G., "A Model for End Milled Surface Topography," *Transactions of the North American Manufacturing Institution of SME*, Vol. 13, pp. 362-368, 1985.

2) Babin, T. S., Sutherland, J. W., and Kapoor, S. G., "On the Geometry of End Milled Surfaces" *Transactions of the North American Manufacturing Institution of SME*, Vol. 14, pp. 168-176, 1986.

3) Goto, H., and Sasaoka, T., "Vertical Micro Positioning System Using PZT Actuators," *Bulletin of the Japan Society of Precision Engineering*, Vol. 22, pp. 277-282, 1988.

4) Hara, Y., Montishi, S., and Yashida, K., "A New Micro-Cutting Device with High Stiffness and Resolution," *Annals of the CIRP*, Vol. 39, pp. 375-378, 1990.

5) Hong, M. S., and Ehmann, K. F., "Practical Implementation of Tertiary Cutter Motions for the Improvement of 3-D Sculptured Surface Characteristics in Milling," *Transactions of the North American Manufacturing Institution of SME*, Vol. 18, pp. 222-229, 1990.

6) Hong, M. S., "Generation, Characterization and Synthesis of Engineering Surfaces," *Ph.D. Thesis*, Northwestern University, Evanston, Illinois, U.S.A., 1994.

7) Katoh, T., Tsuda, N., and Sawabe, M., "One Piece Compound Parallel Spring with Reduction Flexure Levers," *Bulletin of the Japan Society of Precision Engineering*, Vol. 18, pp. 329-334, 1984.

8) Mitzutani, K., Kawano, T., and Tanaka, Y., "A Piezoeletric-Drive Table and Its Application to Micro-Grinding of Ceramic Materials," *Precision Engineering*, Vol. 12, pp. 219-226, 1990.

9) Moriyama, S., Harada, T., and Takanashi, A., "Precision X-Y Stage with a Piezo-driven Fine-table," *Bulletin of the Japan Society of Precision Engineering*, Vol. 22, pp. 13-17, 1988.

10) Paros, J., and Weisbord, L., "How to Design Flexure Hinges," *Machine Design*, Vol. 37, pp. 151-156, 1965.

11) Patir, N., and Cheng, H. S., "An Average Flow Model for Determining Effects of Three Dimensional Roughness on Partial Hydrodynamic Lubrication," *Trans. of ASME, J. of Lubrication Engineering*, Vol. 100/1, pp. 12-18, 1978.

12) Rasmussen, J. D., Tsao, T. C., Hanson, R. D., and Kapoor, S. G., "A Piezoeletric Tool Servo System for Variable Depth of Cut Machining," *Trans. of ASME, Precision Machining*, Vol. 58, pp. 119-129, 1992.

13) Scire, F., and Teague, C., "Piezodriven 50-μm Range Stage with Subnanometer Resolution," *Review of Scientific Instruments*, Vol. 49, pp. 1735-1740, 1978.

14) You, S. J., and Ehmann, K. F., "Synthesis and Generation of Surfaces Milled by Ball Nose End Mills Under Tertiary Cutter Motion," *Trans. of ASME, J. of Engineering for Industry*, Vol. 113, pp. 17-24, 1991.

15) Zhong, Z., and Nakagawa, T., "Precision Grinding of Curved Surface Using a Displacement Table," *Annals of the CIRP*, Vol. 40, pp. 305-315, 1991.